Reusable Device for the Electrical Sensing of Red Blood Cells Rigidity Abnormalities, Based on A Reversible Microfluidic Assembly*

Tieying Xu, Maria A. Lizarralde-Iragorri, Jean Roman, Emile Martincic, Valentine Brousse, Wassim El Nemer, Olivier Français, and Bruno Le Pioufle

Abstract— **Combining microfluidic with sensors enables the development of smart analysis systems. Microelectrodes can be embedded within the microchannels network for electrical sensing, electrochemical analysis or impedance measurement. However, at the laboratory scale, the assembly between microfluidic network and electrical parts on the substrate remains an issue. This paper first discusses the principles of biosensing, and then proposes an original device integrating microfluidics with microelectrodes for the analysis of red blood cells transit in a structure mimicking micro-vascular flow. Some results concerning red blood cells discrimination of sickle cell disease are discussed with statistical analysis.**

Clinical Relevance— **This paper introduces a portable reusable device combining a microfluidic blood vessel mimicking network with microelectrodes for the biosensing of RBC.**

I. Introduction

Sickle cell disease is determined by genetic abnormalities causing hemoglobin polymerization under deoxidation condition in red blood cells [1]. This polymerization induces variation of RBC deformability leading to changes in shape from biconcave disk to sickle. As a consequence, the transit time of RBC in blood vessel microcapillaries becomes longer, sometimes causing vaso-occlusive crisis. Statistical analysis of the variation of RBC deformability is currently achieved using an optical microscope [2], by observing RBC shape and calculating the transit time. However, this method lacks of productiveness. Besides such optical analysis, new electrical approaches for faster and further characterization of RBC by their dielectric properties are emerging. In this paper we describe a microfluidic system for the electrical monitoring of RBC transit. However, the assembling of microfluidic and electrical subparts of the system remains difficult, as a micrometer scale alignment is required between those subparts. In this paper, several strategies are presented to overcome this bottleneck, which might be helpful for the future biomedical application of blood disease.

II. Biosensing Principle

As the electrical impedance represents the opposition of the induced current when the system receives a voltage excitation, the microfluidic channel containing cells suspension could also be characterized by its total bioimpedance. The complex permittivity ε^* of such microfluidic channel, which depends on the material (the cell cytoplasm, the cell membrane, the medium, the volume fraction of the cell within the medium and the Claussius-Mossotti factor f_{CM}), is represented by the permittivity ε and the conductivity σ :

$$\varepsilon^* = \varepsilon - i\frac{\sigma}{\omega} \qquad (1)$$

By considering the Maxwell mixture theory [3], the total bioimpedance Z could be represented by the equation:

$$Z(\omega) = \frac{D}{S}\frac{1}{i\omega\varepsilon^*} \qquad (2)$$

Where ω represents the angular frequency of the electrical excitation sent to the microfluidic channel, D represents the distance between the electrodes, S represents the surface of the electrode. The total impedance of the system could be thus calculated (See Figure 1.A., Cdl: double layer capacitance, Rsol and R'sol: solution resistance, Cmemb: RBC membrane capacitance, Rcyto: RBC cytoplasm resistance).

III. Experimental

The microfluidic channels network contains 8 zones of 24×10 microcapillaries matrix (24 branches in parallel and 10 microcapillaries in series) (Figure 1.B.). Each microcapillary (length= 130µm) has a symmetric structure by reducing the width from 20µm to 10µm and finally to 5µm. All the microcapillaries have a height of 2µm. The microfluidic channels network has been fabricated by casting PDMS from a trilayer SU8 mold to induce repetitive mechanical stress to RBCs during their transit in the microcapillary. RBCs were characterized electrically by a pair of gold electrodes (Cr 20nm/Au 200nm), which was obtained by wet etching

method, placed beside the third microcapillary (or restriction) of external branch of the array. That electrical signal provides several information like transit time and blockade amplitude due to the RBC transiting in single microcapillary (Figure 1.A., B.). This information is recorded for each cell transit and then translated to a consistent statistical result (control or SCD patient) by studying the value distribution.

Concerning microfluidic devices based on Polydimethylsiloxane material (PDMS), the conventional irreversible bonding using oxygen plasma treatment (300W, 300mTorr, 20s) was firstly assessed (Figure 2.A.). "-CH3" terminal groups of Polydimethylsiloxane (PDMS) are replaced the hydroxyl group "-OH". Besides, "Si-O" groups of the quartz substrate are replaced by "Si-OH" group. The "Si-O-Si" covalent bond between the PDMS chip and the quartz substrate is then generated by the reaction between two "Si-OH" groups. The microchannels were thus assembled covalently and therefore permanently with the electrodes [4].

This process posed reliability issues due to the difficulty of the alignment between subparts. In addition, the chips can only be used once in this case because of the difficulty to clean for reuse.

A. Fluidic access to electrodes

In order to overcome the alignment problem, another solution was to use external electrodes (needle type) by modifying the fluidic topology with specific channels for the electrical measurement. Thus, fluidic accesses have been placed in order to replace the golds electrodes layer on the quartz substrate. This method eliminates the alignment step between the gold electrodes and the microchannel of PDMS chip. Copper (Cu) needles were used, being inserted at the inlets of the fluidic accesses (Figure 2.B.).

Main drawback was the significant electrical resistance introduced by the fluidic deviation, which reduces the sensitivity of the measurement. Some cells were also deviated by the flow within the fluidic accesses. This method has not been shown to be optimal for measuring the change in impedance due to cell presence in fluidic accesses to electrodes.

B. Depressurization zone around the microfluidic network

A second strategy was tried, where the PDMS subpart of the microdevice was maintained on the quartz substrate, once aligned with gold electrodes, using a depressurization zone around the microchannels (Figure 2.C.). During the experiments, a depressurization around 1bar was applied at the outlet of the dedicated microfluidic network.

This method for the assembly between microfluidic part and electrical part was efficient. But air bubbles appeared due to the gas permeability of PDMS.

C. Assembly by depression: use of parylene deposit

To facilitate not only the alignment between the microchannel and the gold electrodes but also to obtain a reusable microfluidic device, a new assembly method has been developed. To realize the alignment, the PDMS chip containing microfluidic network was rendered impermeable to gases by depositing a thin layer of parylene C (thickness = 3.5μm) [5]. To obtain such parylene layer, parylene C dimers

(7g) were evaporated at 175°C, then pyrolyzed at 690°C, before being deposited of the microdevice (room temperature, 30mbar).

Thanks to this covering layer, the penetration of air across the PDMS chip, was prevented. The capability of the device to flow the cell medium without any gas bubble, due to a packaging by depressurization (-250 mbar), was validated using a colored conductive solution. A comparison between the PDMS chip without the parylene layer and with the parylene layer is presented in figure 2.D.

The alignment of the microchannel and the electrodes was realized before the experiment under an optical microscope (magnification equals to 5×) and readjusted if necessary taking benefits of the reversible assembly.

D. Comparison between two measuring devices: external electrodes and electrodes integrated into the device

A comparison of the impedance characterization, by using Cu vertical electrodes inserted at the entrance of fluidic access (Figure 2.B.) and by using flat gold electrodes aligned with the restrictions (Figure 2.A, C, D.), was realized. All impedance measurements were taken on the third restriction in the external branch. The spectrum of the modulus of the impedance was obtained using the HP 4194A impedancemeter.

The chips were first measured without any conductive solution in the microcapillaries array. This measurement allows us to know the maximum of the device capacity as well as the value of the parasitic capacitance of the chips associated with its electronic measuring system (Figure 3.A.). This phenomenon is similar for both of device assembly. This parasitic effect limits the impedance range of measurement for the restriction.

Two different concentrations of KCl solution were used to fill the microfluidic restrictions. Between the two devices, the spectrum of the impedance modulus is different (Figure 3.A.). Compared to the flat gold electrodes, an increase in total impedance appeared because of the external integrated electrodes (Cu) inserted into the fluidic access.

At low frequencies ($<10^3$Hz), a slope related to the effect of the double layer capacitance was observed in the case of thin gold electrodes. An optimal frequency of the excitation could be extracted between 10^3Hz and 10^5Hz. A decrease in the modulus of the impedance was found with the increase in the concentration of the KCl solution ((w/v)% increases from 1 to 5).

With the method of using the microfluidic chip by depression and the use of a parylene layer (see Figure 2.D.), the integrated gold electrodes were chosen thanks to the accuracy of the impedance measurement at the working frequency. The filling of the restriction was carried out by solutions of different conductivities (Figure 3.B.).

To choose the optimal work frequency between 10^3Hz and 10^5Hz, the distinction between two different conductive solutions of KCl was observed: the restriction filled by the solution of 630μS/cm and 14.41mS/cm. With the consideration of the double layer capacity effect, the parasitic capacity effect as well as measurement resolution, 10^4Hz was

chosen to be the optimization of electrical excitation frequency.

E. Electrical sensing for RBCs transit within the microcapillary

The experiments were carried out with the injection of RBCs suspension of 2% hematocrit by depressurization (-250mbar) and the electrical sinusoidal excitation (2V, 10^4Hz) within the restriction. At the same time, optical monitoring for RBC transit was permitted.

The discrimination between normal RBCs (from one control person) and sickle cells (from the patient having sickle cell disease) was achieved by the comparison of transit time and blockade amplitude obtained by the numerical electrical signal extraction. A sum of Gaussian distribution fitted with the histogram of each physical parameter was calculated for both normal RBCs (535 cells) and SCD RBCs (538 cells) population. That allows us to achieve the mean value and variance (see Table I.).

IV. RESULTS AND DISCUSSION

The comparison of deformability capacity to pass through the restriction was realized between control RBCs and the RBCs affected by sickle cell disease (SCD). The loss of deformability of SCD cells and the increase of cell rigidity cause an increasing of the transit time ($\mu_t < \mu_{SCD\_t}$, see Figure 4.A. and Table I.). At the same time, its dispersion indicates the RBC deformability variation caused by such genetic sickle cell disease ($\sigma_t^2 < \sigma^2_{SCD\_t}$).

Due to cell dehydration, the SCD cells change from biconcave shape to sickle shape inducing a smaller contact surface with the microcapillary wall. At the same time, the SCD cell elongation is more important than normal cell and cells are more rigid that might induce a blockade amplitude more important. However, when SCD RBC squeezed into the restriction, its longitudinal axis was in front of the flow direction [6]. That could also explain the smaller blockade amplitude comparing to the control RBC. These factors are observed and confirmed by a morphologic study under optical microscope. Both of them influence the blockade amplitude results (Figure 4.B.). The main SCD RBCs subpopulation has a blockade amplitude less important than control RBCs population ($\mu_a < \mu_{SCD\_a}$, see Figure 4.B. and Table I.). Irreversibly sickled cells (ISCs) were observed at the end of the 10 restrictions branch.

The scatter plot representing the blockade amplitude versus the transit time, for 535 control RBCs and 538 SCD RBCs was also realized. A distinction between SCD cells and normal cells can then be achieved (See Figure 4.C.).

TABLE I.   MEAN VALUE AND VARIANCE OF THE TRANSIT TIME O BLOCKADE AMPLITUDE FOR CONTROL RBCS AND SCD RBCS.

		μ		**σ²**
Control RBCs transit time	μ_t	0.0072 ± 6e-5s	σ_t^2	2.1e-6 ± 3.6e-9s^2
SCD RBCs transit time	μ_{SCD_t}	0.0078 ± 0.0001s	$\sigma^2_{SCD\_t}$	3.6e-6 ± 1.5e-8s^2
Control RBCs blockade amplitude	μ_a	0.002 ± 2.6e-5V	σ_a^2	3.6e-7 ±1.6e-9V^2
SCD RBCs blockade amplitude	μ_{SCD_a}	0.0011± 1.9e-5V	$\sigma^2_{SCD\_a}$	1.14e-7 ± 4.65e-10 V^2
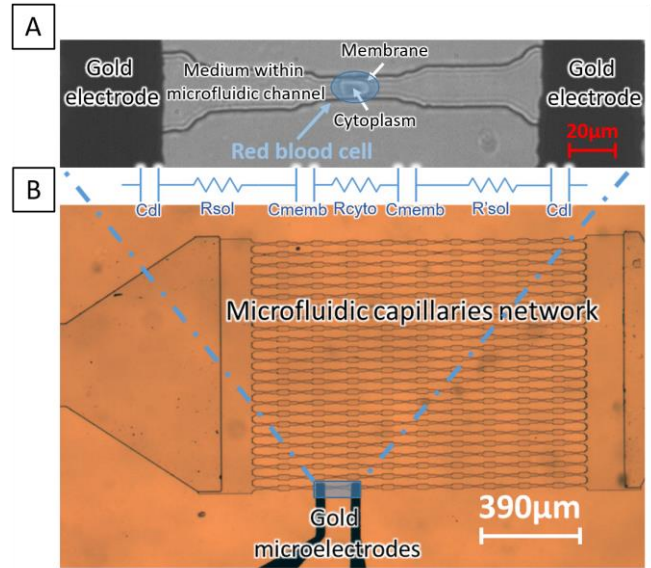
Figure 1. A. Red blood cell transit in the microrestriction and equivalent circuit of total system for bioimpedance monitoring; B. Microfluidic capillaries (or restrictions) network of 24×10.
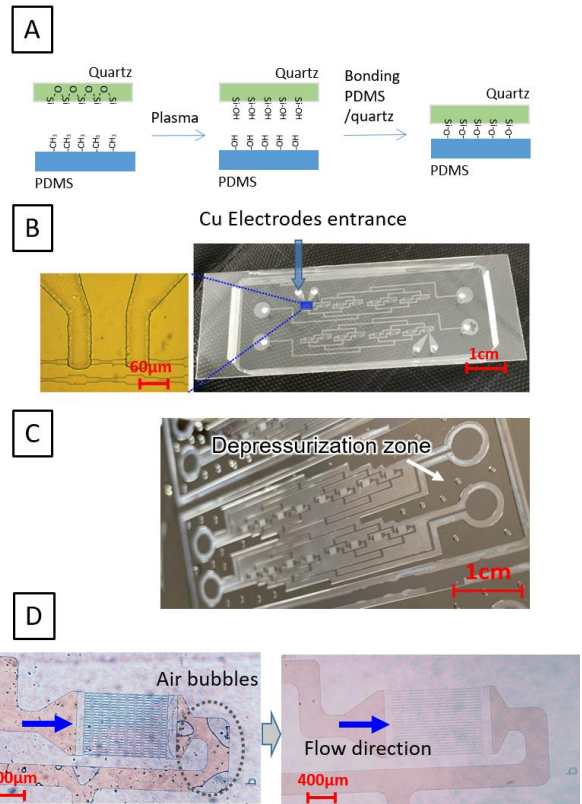
Figure 2. A. Principle of the irreversible bonding by oxygen plasma; B. Fluidic access to electrodes; C. Depressurization zone around the microfluidic network; D. Assembly by depression: use of parylene deposited layer.
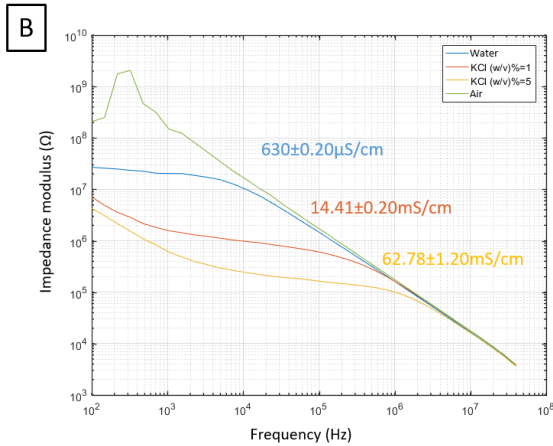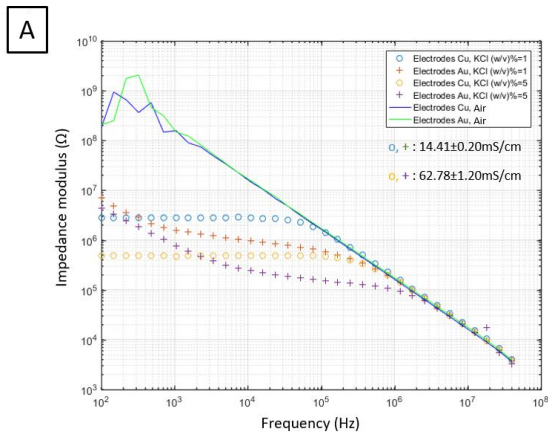
Figure 3. A. Impedance modulus spectrum of KCl solution of different concentrations; B. One single restriction impedance modulus spectrum.
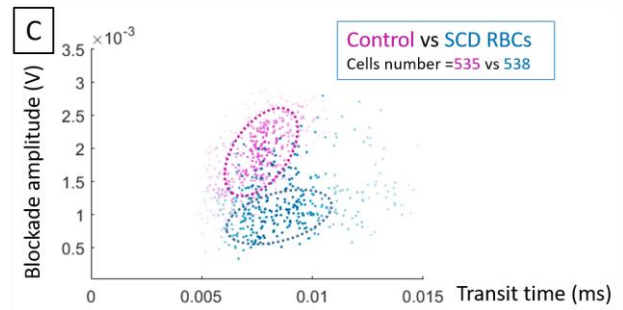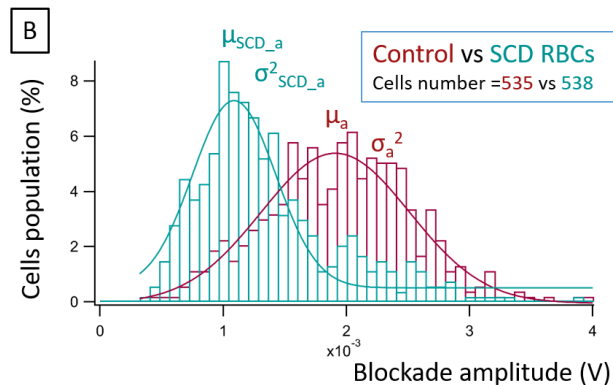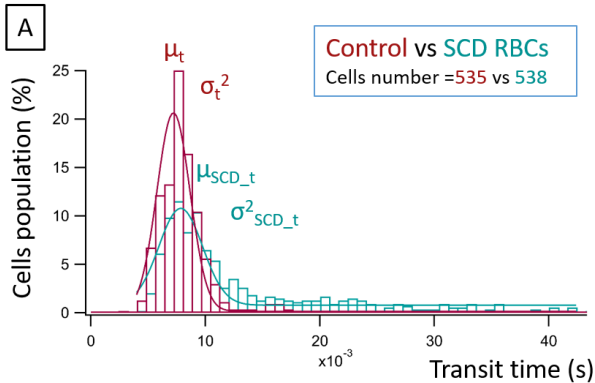
Figure 4. A. Comparison of the transit time between Control RBCs and SCD RBCs; B. Comparison of the blockade amplitude between Control RBCs and SCD RBCs; C. Scatter plot representing the blockade amplitude versus the transit time, for Control RBCs and SCD RBCs.

V. CONCLUSION

In this paper, four different assembly methods between microfluidic and electrical part were discussed. With the consideration of specific experimental conditions, their advantages as well as disadvantages were analyzed. In the case of electrical monitoring of RBC transit, instead of using an irreversible assembly by O_2 plasma, thanks to the supplementary layer of parylene, a reversible assembly was proposed.

Physical parameters like the RBC transit time and the blockade amplitude were obtained by electrical signature analysis and verified by optical monitoring. Discrimination between RBCs from healthy person and patient of sickle cell disease was achieved. Such assembly shows its feasibility for the detection of RBC pathology as well as drug screening to RBC genetic disorders. That would be the first step of 2D biosensing mapping for cells diagnostic.

REFERENCES

[1]   L. Pauling, H. A. Itano, S. J. Singer, and I. C. Wells, "Sickle Cell Anemia, a Molecular Disease," *Science (80-.).*, vol. 110, no. 2865, pp. 543–548, Nov. 1949.

[2]   J. C. Pinder and W. B. Gratzer, "Structural and Dynamic States of Actin in the Erythrocyte," no. March, 1983.

[3]   G. A. Niklasson, C. G. Granqvist, and O. Hunderi, "Effective medium models for the optical properties of inhomogeneous materials," *Appl. Opt.*, vol. 20, no. 1, p. 26, 1981.

[4]   A. Iles, "Plasma Treated PDMS for improved bonding performance of microfluidic devices," 2017.

[5]   S. Pursel, M. W. Horn, M. C. Demirel, and A. Lakhtakia, "Growth of sculptured polymer submicronwire assemblies by vapor deposition," *Polymer (Guildf).*, vol. 46, no. 23, pp. 9544–9548, Nov. 2005.

[6]   T. Xu *et al.*, "Characterization of red blood cell microcirculatory parameters using a bioimpedance microfluidic device," *Sci. Rep.*, vol. 10, no. 1, p. 9869, Dec. 2020.